DOI: 10.1002/ente.201800091

Use the Indirect Energy Conversion of the Phosphor Layer to Improve the Performance of Nuclear Batteries

Zhengrong Zhang,[a] Xiaobin Tang,*[a, b] Yunpeng Liu,[a, b] Dayong Zhou,[c] Zhiheng Xu,[a] Min Wu,[c] and Zhangyi Cao[c]

The GaAs X-ray nuclear battery without and with the phosphor layer was investigated under the irradiation of the X-ray tube. The output power was significantly improved by introducing ZnS:Cu or (Zn,Cd)S:Cu phosphor layer, but not by ZnS:Ag phosphor layer because of the degree of spectral matching between the phosphor layer and the GaAs device. To analyze the radioluminescence (RL) effects of the phosphor layers under X-ray excitation, we measured the RL spectra of the different phosphor layers. The RL spectra of the different phosphor layers revealed their fluorescence in the wavelength range of approximately 375–675 nm. Light at the exact wavelength can be used by the GaAs device to produce electricity. Considering irradiation damage of ZnS:Cu phosphor layer induced by X-rays, an additional experiment was carried out to examine irradiation damage of ZnS:Cu. The results indicate that irradiation effect on the RL performance of ZnS:Cu was not obvious.

Introduction

Nuclear batteries have potential uses as power supplies in micro-electromechanical systems (MEMS) due to their high energy density, stability, and long life.[1–4] For these reasons, they have received considerable research attention.[5] As a representative type of nuclear batteries, X-ray nuclear batteries are attracting widespread interest because of their excellent properties.[6–8] Compared to alpha and beta sources, the use of X-ray source can reduce device damage risks in the semiconductor, resulting in a substantially increased nuclear battery lifetime.[7,9] In addition, X-ray can be shielded easier than γ-ray because of the low-energy photons emitted from the source.[9,10] Recently, the electron capture X-ray emitter ^{55}Fe has received research attention for nuclear microbattery use.[9] X-ray battery is a promising candidate for use as a power supply in MEMS based on above-mentioned reasons.

GaAs devices are directly sensitive to X-ray radiation, although their sensitivities are poor because X-ray photons can pass through the thin photovoltaic material without imparting all of its energy.[11] To exploit the X-ray energy to a greater extent, this article introduced the phosphor layer into the GaAs X-ray nuclear battery. A schematic presentation of the operating principle of the GaAs X-ray nuclear battery without and with phosphor layer is shown in Figure 1.

As illustrated in Figure 1a, the battery is composed of two parts: an X-ray source and a GaAs device. The battery can convert the kinetic energy of the X-ray photons to electricity via a GaAs photovoltaic material. In Figure 1b, the battery is composed of an X-ray source, phosphor layer, and GaAs device. In this battery, the phosphor layer can absorb the X-ray energy emitted from X-ray emitter and produce radioluminescence (RL). The GaAs photovoltaic material receives RL and creates many electron-hole pairs (EHPs). In addition, other EHPs are also generated when X-ray photons pass through the phosphor layer into the GaAs device. All these EHPs are then separated by a built-in electrical field. Finally, the battery delivers an output current after being connected to an external circuit.[12–14]

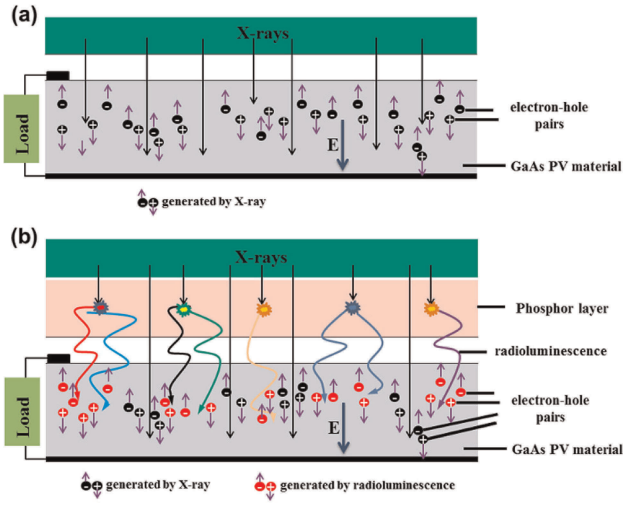

Figure 1. Schematic representation of a GaAs X-ray nuclear battery (a) without and (b) with the phosphor layer.

[a] Z. Zhang, Prof. X. Tang, Dr. Y. Liu, Z. Xu
Department of Nuclear Science and Engineering
Nanjing University of Aeronautics and Astronautics
29 General Road, Jiangning District, Nanjing 211106, China
E-mail: tangxiaobin@nuaa.edu.cn
[b] Prof. X. Tang, Dr. Y. Liu
Jiangsu Key Laboratory of Material and Technology for Energy Conversion
Nanjing 211106, China
[c] D. Zhou, M. Wu, Z. Cao
Shanghai Institute of Space Power Sources
Shanghai 200245, China

Supporting information for this article is available on the WWW under https://doi.org/10.1002/ente.201800091

The objective of this research is to investigate the characteristics of X-ray nuclear battery before and after introducing a phosphor layer by using X-rays of different energies. The optical properties of luminescent materials and the degree of spectral matching between the phosphor layers and GaAs device were analyzed. There was a good match between the RL spectra of ZnS:Cu or (Zn,Cd)S:Cu phosphor layer and the spectral response curves of the GaAs device. The RL released from ZnS:Cu and (Zn,Cd)S:Cu can increase the output power of the battery to a significant extent. Moreover, we investigated the radiation effects on the ZnS:Cu luminescent material irradiated by different doses of ^{60}Co γ-rays.[15,16] The results of this research indicate that there is no obvious variation of RL efficiencies with the increase of irradiation dose.

Results and Discussion

Electrical performances of the X-ray nuclear battery without the phosphor layer

Tube currents were set to 100–800 μA and the tube voltages were set to 10, 15, 20, 25, and 30 kV, respectively. The electrical performances of the X-ray nuclear battery without phosphor layer were measured during continuous and direct X-ray exposure. The corresponding *I–V* characteristics were obtained with a dual-channel system source meter instrument (Keithley Model 2636 A, USA) and all of them are illustrated in Figure 2. It can be seen that both I_{sc} and V_{oc} increased significantly as increasing tube current under different tube voltages.

Figure S1 shows the changes in I_{sc}, V_{oc}, P_{max}, and *FF* for the X-ray nuclear battery without phosphor layer as a function of tube current (100–800 μA). Corresponding changes in the electrical performances were observed after the tube current was increased (Figure S1). Obvious increases in the I_{sc}, V_{oc}, P_{max}, and *FF* values were observed and the values of these electrical parameters reach a maximum at tube currents of up to 800 μA. The rise velocity of I_{sc} and P_{max} was faster than that of V_{oc} and *FF*. In Figures S1b and d, the speed of V_{oc} and *FF* values growth became slow with increasing the tube current at different tube voltages.

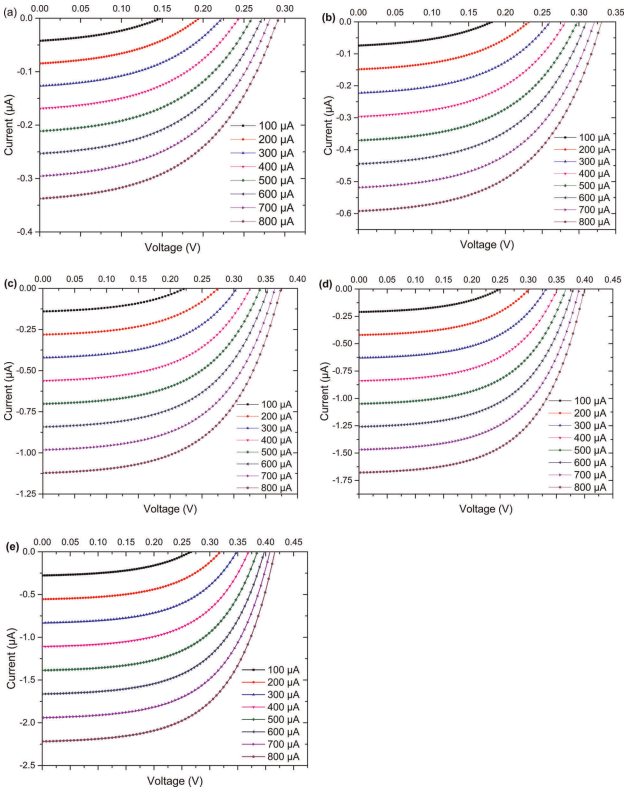

Figure 2. *I–V* curves of the battery under different tube voltages: (a) 10 kV, (b) 15 kV, (c) 20 kV, (d) 25 kV, and (e) 30 kV.

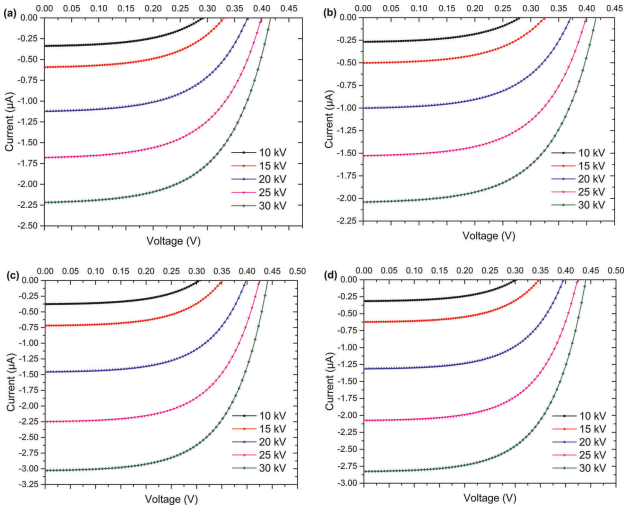

Figure 3. *I–V* curves of the X-ray nuclear batteries: (a) without phosphor layer, (b) ZnS:Ag phosphor layer, (c) ZnS:Cu phosphor layer, and (d) (Zn,Cd)S:Cu phosphor layer.

Electrical performances enhanced by phosphor layer

Considering the X-ray utilization and the final performance output of battery, the ZnS:Ag, ZnS:Cu, and (Zn,Cd)S:Cu phosphor layers were introduced into the X-ray nuclear battery, respectively. In the research, the tube current was set to 800 μA, and the tube voltages were set to 10, 15, 20, 25, and 30 kV, respectively. As shown in Figure 3, it can be seen that I_{sc} and V_{oc} increase significantly with increasing the tube voltage.

Figure 4 shows the changes in I_{sc}, V_{oc}, P_{max}, and *FF* for the X-ray nuclear batteries without and with phosphor layer as a function of tube voltage (range of 10–30 kV). Obviously, I_{sc}, V_{oc}, P_{max}, and *FF* increase significantly with the increase of tube voltage. The I_{sc} and P_{max} values of the battery with ZnS:Cu or (Zn, Cd)S:Cu phosphor layer were greater than those of the battery without phosphor layer. In Figures 4b and d, the V_{oc} and *FF* values of the battery with ZnS:Cu were extremely close to those of the battery with (Zn, Cd)S:Cu,

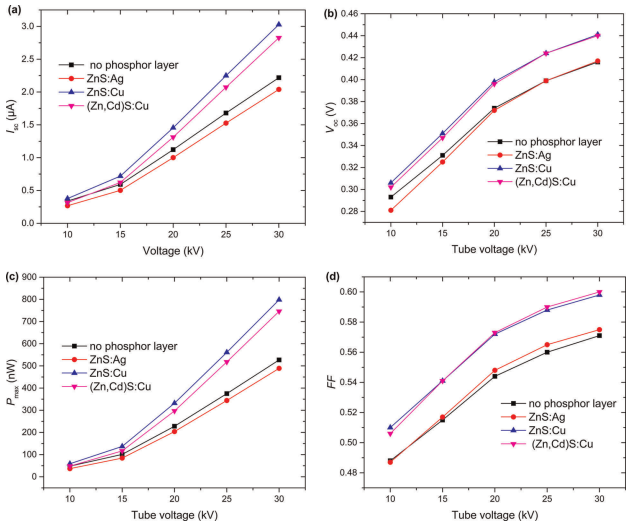

Figure 4. Electrical properties of the X-ray nuclear batteries as a function of X-ray tube voltage: (a) short circuit current I_{sc}, (b) open circuit voltage V_{oc}, (c) maximum power P_{max}, and (d) fill factor *FF*.

Table 1. P_{max} values of batteries without and with phosphor layer.

Tube voltage (kV)	P_{max} Without phosphor layer	ZnS:Ag	ZnS:Cu	(Zn,Cd)S:Cu
10	48	37	59	48
15	101	84	136	117
20	228	203	331	298
25	375	344	560	518
30	527	489	797	745

and were greater than the values of the battery without phosphor layer. Unexpectedly, I_{sc} and P_{max} values of the battery coupled with ZnS:Ag were smaller than those of the battery without that, respectively.

Figure 5 shows the comparison chart of the P_{max} of the batteries without and with phosphor layer under different tube voltages. The P_{max} values of the batteries are listed in Table 1. As shown in Table 1, P_{max} values of the batteries with ZnS:Cu or (Zn,Cd)S:Cu phosphor layer increase significantly at different tube voltages. Especially for the tube voltage of 30 keV, P_{max} increased by 51.23 % and 41.36 %, respectively, after loading ZnS:Cu and (Zn,Cd)S:Cu phosphor layers. However, P_{max} of the battery with ZnS:Ag phosphor layer decreased by 7.21 % under 30 keV tube voltage. This is because the phosphor layer blocked the X-ray photons and reduced their energies. In other words, the X-ray photons energies were reduced to some extent when X-ray photons get through phosphor layer into the GaAs device. The RL effect of the phosphor layer was stronger than it's X-ray-blocking capability for the batteries with ZnS:Cu or (Zn,Cd)S:Cu, while this phenomenon was inverse for the battery with ZnS:Ag.

Optical performances of the phosphor layers

In order to clarify the differences in performance among the ZnS:Ag, ZnS:Cu, and (Zn,Cd)S:Cu phosphor layers, experiments were carried out using a Cary Eclipse fluorescence spectrophotometer (Agilent Technologies G9800a, Malaysia). Figure 6 shows the RL spectra of the ZnS:Ag, ZnS:Cu, and (Zn,Cd)S:Cu phosphor layers under different tube voltages, then the tube current was set to 800 μA . The RL relative intensities of the phosphor layers were enhanced when the tube voltage increased. However, the emission peak wavelengths of ZnS:Ag, ZnS:Cu, and (Zn,Cd)S:Cu, which were approximately 450, 530, and 560 nm respectively, remained steady and unchanged at different tube voltages.

The RL spectra of ZnS:Ag, ZnS:Cu, and (Zn,Cd)S:Cu phosphor layers at the same tube voltage are all shown in Figure S2. The phosphor layers exhibited different emission

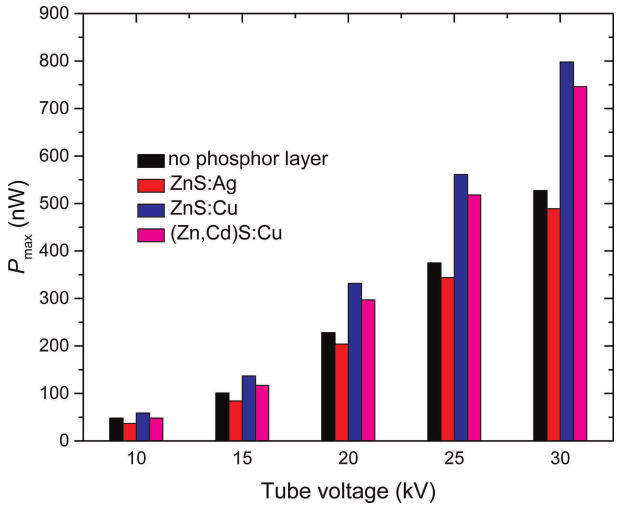

Figure 5. Maximum output power comparison chart for X-ray nuclear batteries without and with phosphor layer under different X-ray excitation conditions.

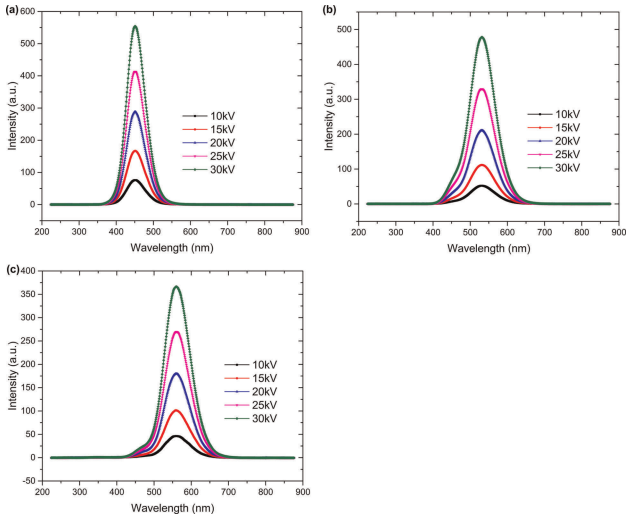

Figure 6. RL spectra of phosphor layers under different tube voltages: (a) ZnS:Ag, (b) ZnS:Cu, and (c) (Zn,Cd)S:Cu.

spectra because of the presence of different luminescent materials. It can be seen that the phosphor layers emit fluorescence at wavelength range of 375–675 nm. The RL intensities of the ZnS:Ag, ZnS:Cu, and (Zn,Cd)S:Cu phosphor layers were weakened when the phosphor layers were subjected to the same excitation conditions. This phenomenon indicated that the ZnS:Ag and ZnS:Cu exhibit higher RL efficiencies than (Zn,Cd)S:Cu under excitation by X-rays.

Degree of spectral matching between the different phosphor layers and GaAs device

The spectral response curves of the GaAs device and the RL spectra of different phosphor layers are given in Figure 7. It can be observed that the external quantum efficiency (EQE) of the GaAs device was 80 %–91 % at a wavelength range of 500–675 nm, where the light was absorbed efficiently by the GaAs device. However, when the phosphor layer emitted RL with a range of 375–450 nm, the EQE of the GaAs device was only 19 %–74 %. Hence, there was a good match between the RL spectra of ZnS:Cu, (Zn,Cd)S:Cu phosphor layers and the spectral response of the GaAs device. The finding indicated that the ZnS:Cu, and (Zn,Cd)S:Cu phosphor layers are more suitable than ZnS:Ag to couple with the GaAs device.

Influences of irradiation on the ZnS:Cu

The irradiation resistance of the GaAs device under X-ray excitation was studied in our previous work and the results showed that the performance of the GaAs device did not significantly change after irradiation.[12] At present, based on the experimental results, we know ZnS:Cu is more suitable than ZnS:Ag for coupling with the GaAs device, and exhibited higher RL efficiency than (Zn,Cd)S:Cu under X-ray excitation. Therefore, ZnS:Cu can be used in X-ray nuclear batteries to improve output performance of batteries and the X-ray irradiation effects on the ZnS:Cu should be carried out. Considering the existing experimental conditions, we use ^{60}Co gamma source as a suitable substitute for X-ray tube to irradiate the ZnS:Cu due to long-term working.

ZnS:Cu samples with the same performance were exposed to gamma irradiation. The irradiation dose rate was 0.69 kGy/h. The irradiation time of ZnS:Cu samples were 0, 10, 20, 30, 40, 50, and 60 hours. The corresponding irradiation doses were 0, 6.9, 13.8, 20.7, 27.6, 34.5, and 41.4 kGy, respectively. Then the ZnS:Cu samples irradiated by different doses were studied by scanning electron microscope (SEM) and X-ray diffraction (XRD).

SEM images of ZnS:Cu irradiated by different doses of γ-rays are shown in Figure S3. It can be seen that each sample has the faceted equiaxed shape and the particle size of less than about 50 μm. All SEM images of samples with various γ radiation doses also show the similar morphology with the sample presented here.

XRD patterns of the ZnS:Cu irradiated by different doses of γ-rays, as shown in Figure 8, reveal the hexagonal wurtzite structure of ZnS:Cu. The narrowness of the peaks is due to the larger particle size of the crystals. Comparing the positions of peaks before and after irradiation, the positions have remained essentially unchanged. The result shows that has little change in ZnS:Cu for transforming from the hexagonal phase (wurtzite) to the cubic phase (zinc blende).

Under X-ray excitation (tube voltage: 30 kV, tube current: 800 μA), the RL spectra of ZnS:Cu phosphor layers irradiated by different doses of γ-rays were measured by using a Cary Eclipse fluorescence spectrophotometer. In contrast, there are no significant changes in the RL intensities of ZnS:Cu phosphor layers before and after irradiation and the maximum emission wavelengths stabilize at 525–530 nm, as shown in Figure 9. The change rates in values of luminescent peaks after irradiation are less than 6 %. In addition, the fluorescence emitted from ZnS:Cu after irradiation was also in the wavelength range of approximately 420–660 nm. Hence,

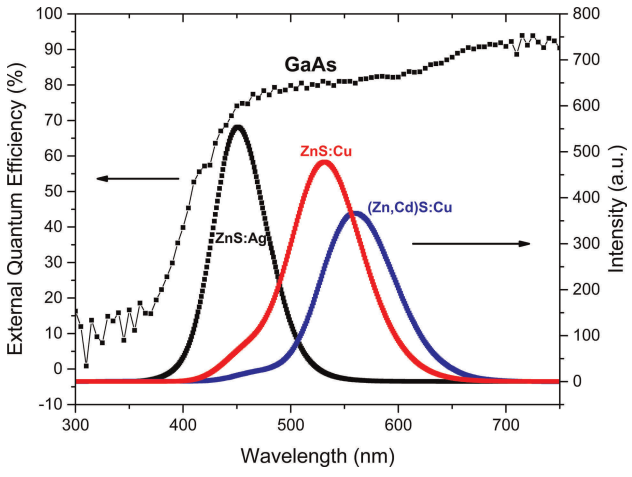

Figure 7. Spectral response curves of the GaAs device and RL spectra of different phosphor layers under excitation of 30 keV X-ray tube voltage.

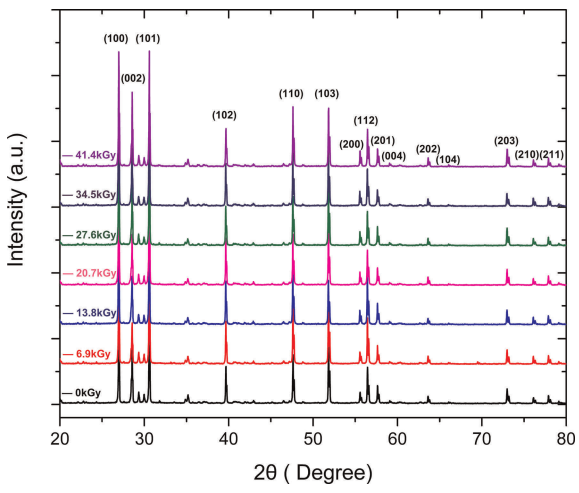

Figure 8. XRD pattern of the ZnS:Cu irradiated by different doses of γ-rays.

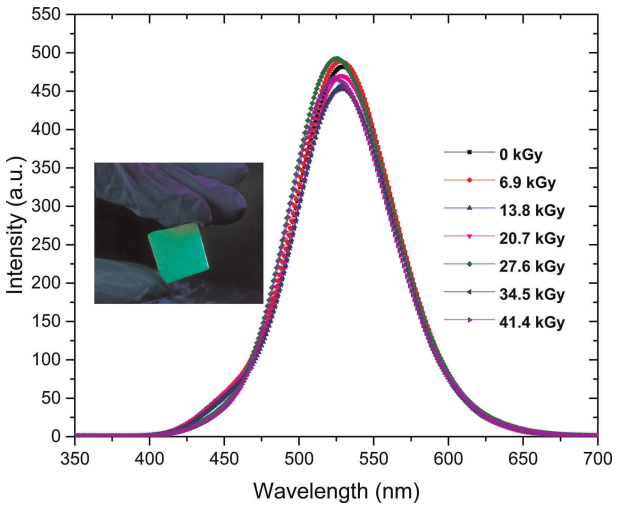

Figure 9. RL spectra of the ZnS:Cu phosphor layers irradiated by different doses of γ-rays.

the irradiation effect on the RL efficiency of ZnS:Cu is little, and ZnS:Cu can be expected to be used for improvement of output power in X-ray battery because of its high resistance to gamma irradiation.

Conclusions

The GaAs X-ray nuclear batteries without and with the phosphor layer were investigated under different energy X-rays. In this proof of concept experiment, the I_{sc}, V_{oc}, P_{max}, and *FF* of battery increase significantly with the increase of tube current under the different tube voltages and the RL relative intensity of phosphor layers increased as the tube voltage increased. Under the same tube voltage, the battery coupled to ZnS:Cu generated the best electric power compared with that coupled to (Zn,Cd)S:Cu or ZnS:Ag. Especially for the tube voltage of 30 keV, P_{max} increased by 51.23 %, after the ZnS:Cu phosphor layer was introduced. This is due to the fact that there is a good match between the RL spectra of ZnS:Cu and the spectral response of the GaAs device, as well as ZnS:Cu exhibited higher RL efficiency than (Zn,Cd)S:Cu under X-ray excitation. Under γ irradiation, even for 41.4 kGy, the ZnS:Cu still has not transformed from the hexagonal phase to the cubic phase and shows the similar morphology compared with the non-irradiated sample. In addition, it was found from the experimental results the changes in the RL efficiency of ZnS:Cu before and after irradiation were little. It is expected that the optimal design of thickness of phosphor layer under different energies X-ray excitation will improve the efficiency of the battery,[23] and this is the work which we will carry out in the future.

Experimental Section

Experimental materials

An X-ray tube (Shanghai KeyWay Electron Company Ltd., KYW900 A, China) was used as a suitable substitute for the low-energy X-ray source due to safety concerns and convenience. The X-ray tube can provide easy adjustment of the intensity of the emitted X-rays for this experimental research. The basic specifications of the X-ray tube used in the present study are listed in Table 2.

Table 2. Specification of the X-ray tube.

Anode voltage	Anode current	Maximum power	Filament voltage	Filament current
50 kV	0–1 mA	50 W	2.0 V	50 kV/1 mA, I_f = 1.7 A
Thickness of the beryllium window	Target angle	Focus spot size	Grounded mode	Target
200 μm	10°	0.1 mm × 0.1 mm	Grounded-cathode	Molybdenum

Three different phosphor layers were fabricated with ZnS:Ag, ZnS:Cu, and (Zn,Cd)S:Cu phosphor powder and the size of each phosphor layer was 2 cm × 2 cm. The thickness of the phosphor layer is 50 μm, and each of them was fully loaded on the surface of GaAs device in the experiment. These different phosphor layers under 254 nm UV lamps are illustrated in Figure 10. The light-emitting colors of the phosphor layers

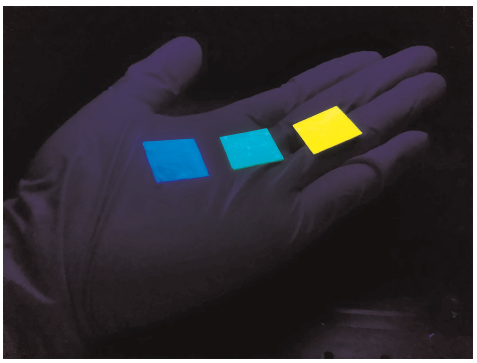

Figure 10. Three different phosphor layers under 254 nm UV lamps (from left to right: ZnS:Ag, ZnS:Cu, and (Zn,Cd)S:Cu phosphor layers).

depend on the material used for preparing phosphor powder. Under UV light, the colors of the phosphor layers were blue, green, and yellow, respectively, as illustrated in Figure 10.

The GaAs device is found to have compact structure,[17] direct band gap structure, high radiation resistance,[18] wide band gap,[19,20] and high crystal quality.[21] For these advantages, the GaAs device was employed as the converter material in the X-ray nuclear battery. The active area of the GaAs device was 10 mm × 10 mm. Figure 11 shows the prototype and internal structure schematic of the GaAs device.

Experimental measurements

Under excitation condition of 10, 15, 20, 25, and 30 kV tube voltages, the X-ray energy spectra were obtained by silicon drift detector (Amptek X-123, USA), as shown in Figure 12. X-ray photons with maximum energy of 30 keV could be found in the figure for the tube voltage of 30 kV. The horizontal and vertical coordinates represent the photon energy and the photon numbers, respectively.

The electrical properties of battery, such as short circuit current (I_{sc}) and open circuit voltage (V_{oc}), were obtained with a dual-channel system source-meter instrument (Keithley Model 2636 A, USA) at room temperature. The maximum output power (P_{max}) and fill factor (FF) can be calculated by Eqs. (1) and (2) as follows:

$$P_{max} = V_{max} \times I_{max} \quad (1)$$

$$FF = \frac{V_{max} \times I_{max}}{V_{oc} \times I_{sc}} \quad (2)$$

where V_{max} and I_{max} are the voltage and current at the maximum power point, respectively.

The RL spectra of different phosphor layers under different tube voltages (10, 15, 20, 25, 30 kV) were tested with a Cary Eclipse fluorescence spectrophotometer (Agilent Technologies G9800a, Malaysia) when the tube current was 800 μA. The data mode of Cary Eclipse luminescence spectrophotometer was set as bio/chemiluminescence, and the emission slit and photomultiplier detector voltage were 20 nm and 800 V, respectively. The spectral response curve of the GaAs device was measured at room temperature by a quantum efficiency spectrometer (Bentham PVE300, Britain). The electrical and optical measurement systems are shown in Figure 13. The experimental set up is shown in Figure 14.

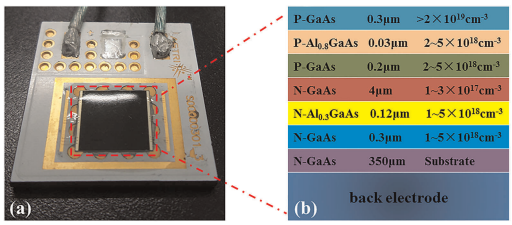

Figure 11. (a) Prototype and (b) internal structure schematic of GaAs device.

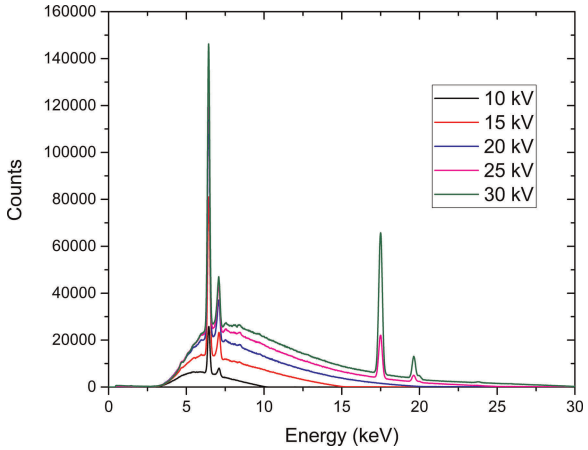

Figure 12. X-ray energy spectrum for a tube voltage of 10, 15, 20, 25, and 30 kV, respectively.

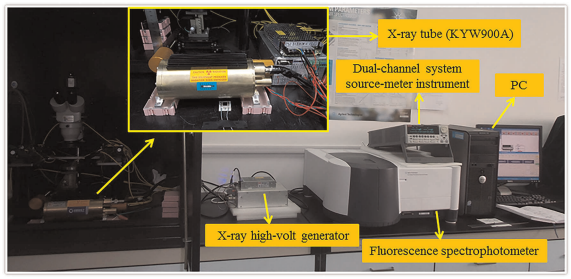

Figure 13. Testing system for electrical performance and optical performance.

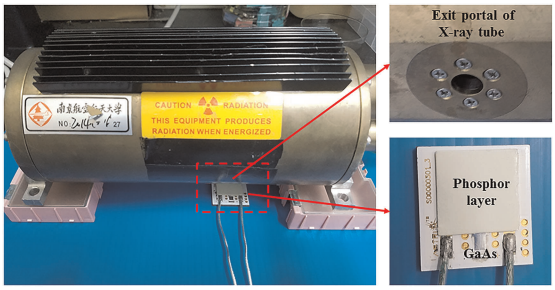

Figure 14. Prototype of the experimental set up enhanced by the phosphor layer.

SEM (Hitachi SU8020, Japan) was used to analyze the micro-morphology of ZnS:Cu before and after irradiation.[22] The phase identification of the corresponding ZnS:Cu was carried out on a XRD system (Bruker AXS D8, Germany).

Acknowledgements

This work was supported by the National Natural Science Foundation of China (Grant Nos. 11675076 and 11505096), the Natural Science Foundation of Jiangsu Province (Grant No. BK20150735), the Funding of Jiangsu Innovation Program for Graduate Education (Grant No. KYLX16_0354), the Shanghai Aerospace Science and Technology Innovation Project (Grant No. SAST2016112) and the Priority Academic Program Development of Jiangsu Higher Education Institutions.

Conflict of Interest

The authors declare no conflict of interest.

Keywords: X-ray nuclear battery · radioluminescence spectra · GaAs device · phosphor layers · irradiation damage

[1] M. A. Prelas, C. L. Weaver, M. Watterman, E. Lukosi, R. Schott, D. Wisniewski, *Prog. Nucl. Energy* **2014**, *75*, 117–148.
[2] Y. P. Liu, X. B. Tang, Z. H. Xu, L. Hong, D. Chen, *Appl. Radiat. Isot.* **2014**, *94*, 152–157.

[3] Z. R. Zhang, Y. P. Liu, X. B. Tang, Z. H. Xu, Z. C. Yuan, K. Liu, W. Chen, *Nucl. Instrum. Methods Phys. Res. Sect. B* **2018**, *415*, 9–16.
[4] J. Russo, M. Litz, W. Ray, G. M. Rosen, D. I. Bigio, R. Fazio, *Appl. Radiat. Isot.* **2017**, *125*, 66–73.
[5] P. B. Koeneman, I. J. Busch-Vishniac, K. L. Wood, *J. Microelectromech. Syst.* **1997**, *6*, 355–362.
[6] G. Lioliou, M. C. Mazzillo, A. Sciuto, A. M. Barnett, *Opt. Express* **2015**, *23*, 21657–21670.
[7] S. Butera, G. Lioliou, A. M. Barnett, *J. Appl. Phys.* **2016**, *119*, 064504.
[8] S. Butera, G. Lioliou, A. B. Krysa, A. M. Barnett, *J. Phys. D. Appl. Phys.* **2016**, *49*, 355601.
[9] G. Lioliou, X. Meng, J. S. Ng, A. M. Barnett, *J. Appl. Phys.* **2016**, *119*, 124507.
[10] S. Butera, M. D. C. Whitaker, G. Lioliou, A. M. Barnett, *Sci. Rep.* **2016**, *6*, 38409.
[11] N. Horiuchi, N. Iijima, S. Hayashi, I. Yoda, *Sol. Energy Mater. Sol. Cells* **2005**, *87*, 287–297.
[12] Z. R. Zhang, X. B. Tang, Y. P. Liu, Z. H. Xu, Z. C. Yuan, K. Liu, W. Chen, *Nucl. Instrum. Methods Phys. Res. Sect. B* **2017**, *398*, 35–41.
[13] X. B. Tang, Z. H. Xu, Y. P. Liu, M. Liu, H. Wang, D. Chen, *Energy Technol.* **2015**, *3*, 1121–1129.
[14] Z. H. Xu, X. B. Tang, Y. P. Liu, Z. R. Zhang, W. Chen, Z. C. Yuan, K. Liu, *Energy Technol.* **2017**, *5*, 1638–1646.
[15] Z. R. Zhang, X. B. Tang, Y. P. Liu, Z. H. Xu, Z. C. Yuan, K. Liu, W. Chen, *J. Radioanal. Nucl. Chem.* **2017**, *312*, 609–614.
[16] M. Liu, X. B. Tang, Y. P. Liu, Z. H. Xu, H. Wang, M. H. Fang, D. Chen, *J. Radioanal. Nucl. Chem.* **2016**, *308*, 631–637.
[17] H. Wang, X. B. Tang, Y. P. Liu, Z. H. Xu, M. Liu, D. Chen, *Nucl. Instrum. Methods Phys. Res. Sect. B* **2015**, *359*, 36–43.
[18] E. Monroy, F. Omnès, F. Calle, *Semicond. Sci. Technol.* **2003**, *18*, R33.
[19] S. M. Sze, K. K. Ng in *Physics of Semiconductor Devices*, John Wiley & Sons, Inc., **2006**, pp. 5–75.
[20] W. J. Choyke, G. Pensl, *MRS Bull.* **1997**, *22*, 25–29.
[21] S. Butera, G. Lioliou, A. M. Barnett, *Appl. Radiat. Isot.* **2017**, *125*, 42–47.
[22] J. H. Park, S. H. Lee, J. S. Kim, A. K. Kwon, L. P. Hong, S. D. Han, *J. Lumin.* **2007**, *126*, 566–570.
[23] M. A. Prelas, M. A. Borass, F. D. L. T. Aguilar, J. D. Seelig, M. T. Tchouaso, D. Wisniewski in *Nuclear Batteries and Radioisotopes*, Springer International Publishing, **2016**, pp. 197–217.

Manuscript received: February 1, 2018
Revised manuscript received: May 9, 2018
Accepted manuscript online: May 12, 2018
Version of record online: August 30, 2018

